Supplementary Information (SI) for Nanoscale.

Supplementary Information (SI†)

Breaking scaling relationship limitations in peroxymonosulfate activation through electronegativity-driven Fe–Mn dual-metal synergy

Table S1	HPLC operating conditions for analyzing various pollutants.
Table S2	EXAFS fitting parameters at the Fe and Mn K-edge for various samples.
Table S3	Comparison of reaction conditions and reaction parameters over the reported DACs, SACs, and nanocatalysts for BPA degradation by PMS activation in the Fenton-like reaction.
Table S4	Parameters of the obtained water samples.
Table S5	The steady-state concentrations and the contribution ratio of various ROS.
Figure S1	SEM images of Fe-Mn DAC.
Figure S2	BPA adsorption on various catalysts in heterogeneous Fenton-like reaction. Reaction conditions: [BPA]=20 mg L^{-1}, [catalyst]=0.2 g L^{-1}, [PMS]=0.2 g L^{-1}, pH=7.0, T=25 °C, adsorption time=30 min.
Figure S3	TOC removal by various catalysts in heterogeneous Fenton-like reaction. Reaction conditions: [BPA]=20 mg L^{-1}, [catalyst]=0.2 g L^{-1}, [PMS]=0.2 g L^{-1}, pH=7.0, T=25 °C, reaction time= 10 min.
Figure S4	PMS consumption with various catalysts for BPA degradation in heterogeneous Fenton-like reaction. Reaction conditions: [BPA]=20 mg L^{-1}, [catalyst]=0.2 g L^{-1}, [PMS]=0.2 g L^{-1}, pH=7.0, T=25 °C, reaction time= 10 min.
Figure S5	Comparison of normalized *k* to metal loading. Reaction conditions: [BPA]= 20 mg L^{-1}, [catalyst]=0.2 g L^{-1}, [PMS]=0.2 g L^{-1}, pH=7.0, T=25 °C.
Figure S6	Comparison of normalized *k* to the molar ratio of metal loading per (a) Fe site and (b) Mn site. Reaction conditions: [BPA]= 20 mg L^{-1}, [catalyst]=0.2 g L^{-1}, [PMS]=0.2 g L^{-1}, pH=7.0, T=25 °C.
Figure S7	Effect of pH on the BPA adsorption in Fe-Mn DAC/PMS system. Reaction conditions: [BPA]=20 mg L^{-1}, [catalyst]=0.2 g L^{-1}, [PMS]=0.2 g L^{-1}, T=25 °C, adsorption time=30 min.
Figure S8	Stability test of Fe-Mn DAC for BPA degradation. Reaction conditions: [BPA]=20 mg L^{-1}, [catalyst]=0.2 g L^{-1}, [PMS]=0.2 g L^{-1}, pH=7.0, T=25 °C, reaction time=30 min.
Figure S9	FTIR spectrum of transmittance of fresh and recycled Fe-Mn DAC.
Figure S10	EPR spectra in PMS alone.
Figure S11	(a) NB, (b) BA, (c) FFA, and (d) *p*-CBA degradation efficiency in Fe-Mn DAC/PMS system. Reaction conditions: Reaction conditions: [BPA]=20 mg L^{-1}, [catalyst]=0.2 g L^{-1}, [PMS]=0.2 g L^{-1}, pH=7.0, T=25 °C , [probe]= 2.0 mg L^{-1}.
Figure S12	*k* of NB, BA, FFA, and *p*-CBA degradation efficiency in Fe-Mn DAC/PMS system. Reaction conditions: [BPA]=20 mg L^{-1}, [catalyst]=0.2 g L^{-1}, [PMS]=0.2 g L^{-1}, pH=7.0, T=25 °C , [probe]= 2.0

	mg L^{-1}.
Figure S13	Linear sweep voltammetry obtained by Fe-Mn DAC as a working electrode in the presence of PMS and BPA.
Figure S14	2-D electron density distribution structure of (a) Fe-SAC, (b) Mn-SAC, and (c) Fe-Mn DAC.
Figure S15	Charge density difference (top view) in a PMS molecule adsorbed on (a) Fe–SAC, (b) Mn-SAC, (c) Fe-Mn DAC $_{\text{(Fe site),}}$ and (d) Fe-Mn DAC $_{\text{(Mn site).}}$
Figure S16	DFT calculations of PMS adsorption and activation on Fe-SAC and Mn-SAC. Representation of PMS molecule, adsorption energy, and O-O bond stretching on (a) Fe-SAC and (b) Mn-SAC, PDOS of (c) Fe-SAC and (d) Mn-SAC.
Figure S17	Bader charges on (a) Fe–SAC, (b) Mn-SAC, (c) Fe-Mn DAC $_{\text{(Fe site)}}$, and (d) Fe-Mn DAC $_{\text{(Mn site)}}$.
Figure S18	Free energy of O transfer in Fe-Mn DAC/PMS system.

1. Materials

Iron(III) chloride ($FeCl_3$, >99%), manganese(II) chloride ($MnCl_2$, >99%), formamide solution (FA), dicyandiamide ($C_2H_4N_4$, 99.0%), zinc chloride ($ZnCl_2$, >99%), bisphenol-A (BPA, ⩾99%), phenol(⩾99%), 4-chlorophenol (4-CP, >99%), 2,4-dichlorophenol (2,4-DCP, 99%), 2,4,6-trichlorophenol (2,4,6-TCP, 99%), sulfamethazine (SMT, >99%), sulfamethazole (SMT, >99%), ofloxacin (OFX, 99%), p-nitrophenol (4-NP, 99%), acetaminophen (AcP, 99%), 4-methoxyphenol (MQ, 99%), 4-bromophenol (BP, 99%), 4-hydroxybenzaldehyde (HBAI, 99%), hydroxybenzoic acid (HBA,99%), o-nitrophenol (2-NP, 99%), ethanol (75%), $2KHSO_5•KHSO_4•K_2SO_4$ (PMS, 42%–46%), benzoic acid (BA, 99%), nitrobenzene (NB, 99%), parachlorobenzoic-acid (*p*-CBA, 99%), furfuryl alchohol (FFA, ⩾99.5%), sodium thiocyanate (NaSCN, 99%), methanol (MeOH, ⩾99%), tert-butanol (TBA, ⩾99.5%), chloroform (CF, ⩾99.5%), potassium iodide (KI, ⩾99%), methyl phenyl sulfoxide (PMSO, 98%), humic acid (HA, >99%), 2,2-azino-bis (3-ethylbenzothiazoline-6-sulfonate) (ABTS, >99%), and boric acid buffer were acquired from Macklin and Aladdin Biochemical Technology Co. Ltd. without further purification.

2. Preparation of Catalysts

NC preparation. $ZnCl_2$ (2.59 g) was dissolved in formamide solution (200 mL) under strong stirring at 30 °C for 1 h to form a homogeneous solution. The resulting solution was then transferred to a Teflon-lined steel autoclave and heated at 180 °C for 12 h, followed by cooling overnight. The resulting precipitate was filtered and washed several times with ethanol and deionized water and dried at 60 °C for 24 h. Subsequently, the precursor was calcined at 900 °C for 2 h under N_2 atmosphere at a heating rate of 5 °C min^{-1} to obtain NC.

Fe-SAC preparation. In the synthesis of Fe-N_4 SAC, $FeCl_3\cdot 6H_2O$ (81.1 mg) and $ZnCl_2$ (2.59 g) were dissolved in formamide solution (200 mL), and the mixture was stirred continuously for 1 h to ensure homogeneity. This homogeneous solution was heated at 180 °C for 12 h in a

Teflon-lined autoclave. After cooling to room temperature, the resulting precipitate was washed with ethanol and DI water and then dried in an oven at 60 °C for 24 h. The dried powder was subsequently calcined at 900 °C at a heating rate of 5 °C min^{-1} for 1 h under N_2 atmosphere to obtain Fe-N_4 SAC.[1]

Mn-SAC preparation. In the synthesis of Mn-N_4 SAC, dicyandiamide (5.0 g) was heated to 550 °C at a rate of 2.5 °C min^{-1} and maintained at this temperature for 4 h in a muffle furnace. After cooling to room temperature, the yellow residue was grinded to obtain C_3N_4. Subsequently, C_3N_4 (0.5 g) and $MnCl_3$ (40.32 mg) were thoroughly grinded in a mortar. The resulting mixture was then calcinated at 550 °C, at a rate of 2.5 °C min^{-1} under N_2 atmosphere for 4 h. Finally, the product was washed with DI water, dried at 60 °C for 12 h, and collected after grinding to obtain Mn-N_4 Mn-SAC.[2]

3. Electrochemical Measurements

An electrochemical workstation (CHI 760E, Chenhua Instrument Co., China) utilizing a three-electrode configuration was used to assess electrochemical impedance spectroscopy (EIS), linear sweep voltammetry (LSV), and current-time (i-t) measurements. The catalysts were coated on a glassy carbon electrode (GCE), serving as the working electrode, while platinum (Pt) and silver/silver chloride (Ag/AgCl) electrodes acted as the counter and reference electrodes, respectively. To prepare the catalyst-modified GCE, 10 mg of the catalyst was dispersed into a mixture of 0.2 mL of 5% Nafion solution, 0.1 mL of isopropanol, and 2.7 mL of DI water. This mixture was then subjected to ultrasonic treatment for 30 min to form a homogeneous catalyst ink. Subsequently, 5 μL of this ink was deposited onto the GCE surface. Before each test, the GCE was polished with alumina slurries on a felt pad, rinsed with DI water, and coated with the catalyst ink. EIS measurements were conducted in an electrolyte composed of 50 mL of BPA solution (20 mg L^{-1}) within a sweep range of 1×10^{-2} to 1×10^{6} Hz. For LSV and i-t measurements, 200 mmol L^{-1} boric acid buffer was used as the electrolyte. The current response at the working electrode was recorded while sweeping the potential from 0.2 to 1.4 V at a scan rate of 10 mV s^{-1}. Additionally, i-t curves for the Fe-Mn DAC electrode were recorded at 0.5 V vs. Ag/AgCl.

4. Determination of PMS consumption

The concentration of PMS remaining in the solution was determined using a colorimetric method. A 0.1 mL reaction sample was collected and filtered through a 0.22 μm filter. Subsequently, 0.4 mL ABTS (10 mM), 0.2 mL Co^{2+} (10 mM), and 9.4 mL DI water were immediately added to the filtered sample and allowed to react for 10 min. This reaction produced a green-colored ABTS radical cation. The resulting solution was then analyzed using a UV/Vis spectrophotometer (UV1800, Shimadzu, Japan) at its maximum absorbance wavelength of 735 nm.[3]

5. Mathematical formulations and calculations

The pseudo-first-order kinetic rate constant (*k*) of the degradation was calculated as follows:

$$-\ln\left(\frac{C_t}{C_0}\right) = kt$$

Where C_0 and C_t represent the initial and the instant concentration of BPA.

The turnover frequency of the degradation was calculated as follows:

$$TOF = \frac{k}{[catalyst]_0}$$

where k is the rate constant of the reaction and $[\mathrm{catalyst}]_0$ is the loading of the catalyst.

The initial reaction rate for metal loading was calculated as follows:

$$k_{\mathrm{MC}} = k/\mathrm{wt\%}$$

Where, k is the initial reaction rate, and MC is wt.% metal loading in the catalyst.[1]

The initial reaction rate per metal site was calculated as follows:

$$k(metal\ site) = \frac{k \times M}{(m \times wt.\%)}$$

Where k is the initial reaction rate, M is the atomic mass of the metal, m is the catalyst mass used in the reaction, and wt.% is the metal loading in the catalyst.[1]

6. Radical probe experiments

In this study, the steady-state concentration of $SO_4^{\cdot -}$, $\cdot OH$, $O_2^{\cdot -}$, and ${}^1O_2$ in the Fe-Mn DAC/PMS system were calculated using BA, NB, *p*-CBA, and FFA as probe compounds. Since the probe compounds were low concentration compared to BPA (20 mg L^{-1} for BPA, 2 mg L^{-1} for BA, NB, FFA, and *p*-CBA), which would not affect BPA degradation.[4] The calculation methods of steady-state concentration of $\cdot OH$, $SO_4^{\cdot -}$, ${}^1O_2$, $O_2^{\cdot -}$ are as follows:

$$(k_{BA,OH\cdot}[\cdot OH]_{ss} + k_{BA,SO_4^{\cdot -}}[SO_4^{\cdot -}]_{ss})t = k_{,BA}t \tag{1}$$

$$(k_{NB,OH\cdot}[\cdot OH]_{ss} + k_{NB,SO_4^{\cdot -}}[SO_4^{\cdot -}]_{ss})t = k_{,NB}t \tag{2}$$

$$(k_{p-CBA,OH\cdot}[\cdot OH]_{ss} + k_{p-CBA,SO_4^{\cdot -}}[SO_4^{\cdot -}]_{ss} + k_{pCBA,{}^1O_2}[{}^1O_2]_{ss} + k_{p-CBA,O_2^{\cdot -}}[O_2^{\cdot -}]_{ss})t = k_{,p-CBA}t \tag{3}$$

$$(k_{FFA,OH\cdot}[\cdot OH]_{ss} + k_{FFA,SO_4^{\cdot -}}[SO_4^{\cdot -}]_{ss} + k_{FFA,{}^1O_2}[{}^1O_2]_{ss} + k_{FFA,O_2^{\cdot -}}[O_2^{\cdot -}]_{ss})t = k_{,FFA}t \tag{4}$$

$k_{BA,OH\cdot}$, $k_{BA,SO_4^{\cdot -}}$, $k_{NB,OH\cdot}$, $k_{NB,SO_4^{\cdot -}}$, $k_{p-CBA,OH\cdot}$, $k_{p-CBA,SO_4^{\cdot -}}$, $k_{pCBA,{}^1O_2}$, $k_{p-CBA,O_2^{\cdot -}}$, $k_{FFA,OH\cdot}$,

$k_{FFA,SO_4^{\cdot -}}$, $k_{FFA,{}^1O_2}$, $k_{FFA,O_2^{\cdot -}}$ values were taken from the literature.[2-3]

The pseudo-first-order reaction rate constant ($k_{,BA}$, $k_{,NB}$, $k_{,p\text{-}CBA}$, $k_{,FFA}$) could be obtained from the slope of the plots of $-ln\frac{[BA]}{[BA]_0}$, $-ln\frac{[NB]}{[NB]_0}$, $-ln\frac{[p-CBA]}{[p-CBA]_0}$, and $-ln\frac{[FFA]}{[FFA]_0}$, respectively. Then, the steady-state concentrations of the reactive species were obtained by solving equations

1-4 and were listed in Table S5.

7. DFT calculations

All theoretical computations were performed using the DFT framework implemented in the Vienna Ab initio Simulation Package (VASP). The Perdew–Burke–Ernzerhof (PBE) generalized gradient approximation was utilized for the exchange-correlation energy, along with the projected augmented wave (PAW) method. Grimme's DFT-D3 method with zero-damping was employed to account for dispersion corrections. For the DFT+U calculations, a magnetic moment of 2.5 was assigned to Fe, while other elements were assigned a moment of 0. A plane-wave basis set with a cutoff energy of 400 eV was used. A 15 Å vacuum layer was incorporated to eliminate interactions between periodic images. For catalyst structure optimizations, the Brillouin zone of the surface unit cell was sampled using Monkhorst–Pack (MP) grids. The convergence criteria were set to 10^{-6} eV for electronic self-consistent iterations and 0.02 eV/Å for atomic forces. A 1×1×1 Monkhorst-Pack grid was used to determine the catalyst surface.

Table S1
HPLC operating conditions for analyzing various pollutants.

Pollutants	**Wavelength**	**Mobile phase (v/v)**
BPA	230	Water : Methanol=30:70
4-CP	280	Water : Methanol=40:60
2,4-DCP	280	Water : Acetonitrile=30:70
2,4,6-TCP	284	Water : Methanol=30:70
HBA	270	Water : Methanol=40:60
HBAI	284	Water : Methanol=50:50
ACP	280	Water : Methanol=20:80
IBP	270	Water : Methanol=40:60
OFX	272	Water : Methanol=40:60
BP	280	Water : Methanol=20:80
MQ	276	Water : Methanol=30:70
Phenol	270	Water : Methanol=35:65

2-NP	280	Water : Methanol=20:80
4-NP	280	Water : Methanol=20:80
SMX	265	Water : Acetonitrile =15:85
SMT	175	Water : Methanol=55:45
NB	265	Water : Acetonitrile=50:50
BA	227	Water : Acetonitrile=50:50
FFA	214	Water : Acetonitrile=50:50
p-CBA	239	Water : Acetonitrile=50:50

Table S2.

EXAFS fitting parameters at the Fe and Mn K-edge for various samples.

Sample	Path	CN^a	R(Å)^b	σ^2 (Å^2)^c	ΔE_0(eV)^d	Range of k	Range of k	R factor
Fe K-edge (S_0^2=0.827)								
Fe foil	Fe-Fe	8.0*	2.475	0.0052	7.0	3.0-14.3	1.0-3.0	0.0019
	Fe-Fe	6.0*	2.854	0.0069				
Fe_2O_3	Fe-O	3.5	1.945	0.0045	-2.4	3.0-13.9	1.0-4.0	0.0064
	Fe-O	2.4	2.110					
	Fe-Fe	4.8	2.961	0.0067				
	Fe-Fe	3.8	3.383					
	Fe-Fe	5.1	3.692					
Fe-Mn DAC	Fe-O	1.6	1.992	0.0105	-1.7	3.0-13.8	1.0-4.0	0.0048
	Fe-N	3.2	2.032					
	Fe-Mn	1.0	2.525	0.0205				
	Fe-Fe	2.5	3.009	0.0060				
	Fe-Fe	3.9	3.524					
Mn K-edge (S_0^2=0.881)								
Mn foil	Mn-Mn	12.0*	2.701	0.0085	11.2	3.0-12.0	1.8-3.0	0.0183
MnO	Mn-O	6.2	2.181	0.0106	-5.7	3.0-13.2	1.0-3.2	0.0062
	Mn-Mn	10.5	3.127	0.0086				
Fe-Mn DAC	Mn-N	3.2	2.051	0.0076	3.9	3.0-10.0	1.0-3.8	0.0047
	Mn-O	1.6	2.073					
	Mn-Fe	1.0	2.520	0.0036				
	Mn-Mn	5.7	3.119		13.3			
	Mn-Mn	4.4	3.304					

^aCN, coordination number; ^bR, the distance between absorber and backscatter atoms; $^c\sigma^2$, the Debye Waller factor value; $^d\Delta E_0$, inner potential correction to account for the difference in the inner potential between the sample and the reference compound; *R* factor indicates the goodness of the fit. $S0^2$ was fixed to 0.827 and 0.881, according to the experimental EXAFS fit of Fe foil and Mn foil by fixing *CN* as the known crystallographic value. * This value was fixed during EXAFS fitting, based on the known structure of Fe and Mn. fitting space: R space; *k*-weight = 3. A reasonable range of EXAFS fitting parameters: $0.800 < S_0^2 < 1.000$; $CN > 0$; $\sigma^2 > 0$ Å^2; $|\Delta E_0| < 15$ eV; R factor < 0.02.

Table S3.
Comparison of reaction conditions and reaction parameters over the reported DACs, SACs, and nanocatalysts for BPA degradation by PMS activation in the Fenton-like reaction.

No.	Catalysts	BPA (mg L^{-1})	PMS (g L^{-1})	Catalyst (g)	k (min^{-1})	TOF $(min\cdot g)^{-1}$	TOF/PMS_0 (L min^{-1} g^{-2})	Reference
1	Fe-Mn DAC	20	0.20	0.20	1.36	6.8	34.0	This work
2	Fe-Co DAC	20	0.40	0.20	0.94	4.7	11.75	[1]
3	Fe-Co DAC	20	0.25	0.20	0.23	1.15	4.60	[5]
4	Fe-Co NC	20	1.20	0.30	0.19	0.63	0.525	[6]
5	Fe-Cu/OPB	20	0.10	0.30	0.025	0.083	0.83	[7]
6	FeSA–N–C	20	0.40	0.15	0.24	1.6	4.0	[8]
7	Fe_1/CN	22.80	0.60	0.50	1.43	2.86	4.77	[9]
8	Cu-N_4/C-B	20	0.40	0.10	0.56	5.6	14.0	[10]
9	Cu–N_4/C	20	0.20	0.10	0.10	1.02	5.10	[10]
10	Co-TPML	11.40	1.20	0.20	0.147	12	10	[11]
11	Co-NC	10.0	0.30	0.05	0.352	7.04	23.47	[12]

12	FeSA-NC	3.0	0.80	0.02	0.24	12	15.0	[13]
13	Co–N_4–C	20	0.20	0.10	0.45	4.52	22.60	[14]
14	NiZn@N–G–900	20	0.20	0.20	0.45	2.67	13.35	[15]
15	10%Ag/C_3N_4	20	0.60	0.10	0.05	0.50	0.83	[16]
16	S–doped C_3N_4	20	0.60	0.10	0.013	0.13	0.217	[17]
17	$CuFe_2O_4$–Fe_2O_3	05	0.70	0.20	1.41	7.05	10.07	[18]
18	DPA–hematite	15	4.0	0.50	0.04	0.08	0.02	[19]
19	Co_3O_4–Bi_2O_3	20	0.20	0.30	0.12	0.4	2.0	[20]
20	$Mn_{1.8}Fe1._{2}O_4$	10	0.40	0.10	0.10	1.0	2.50	[21]
21	$Fe_{0.8}Co_{2.2}O_4$	20	0.40	0.10	0.05	0.5	1.25	[22]
22	O–C_3N_4	12	6.0	0.10	0.065	0.65	0.108	[23]
23	Pd@g–C_3N_4	20	0.60	0.10	0.038	0.38	0.63	[24]

Table S4
Parameters of the obtained water samples.

	Tap Water	**River water**	**Reclaimed water**
pH	7.65	7.40	8.34
HCO_3^- (mg L^{-1})	28.82	63.60	44.14
SO_4^{2-} (mg L^{-1})	41.63	90.65	21.90
PO_3^{4-} (mg L^{-1})	BDL	0.13	0.01
NO_3^- (mg L^{-1})	0.46	8.94	49.91
Cl^- (mg L^{-1})	12.23	94.63	55.71
TOC (mg L^{-1})	-	3.15	4.64

*BDL= Below detection limit

Table S5.

The steady-state concentrations and the contribution ratio of various ROS.

Reactive species	**Steady-state concentration** (M)	**Contribution ratio** (%)
$\cdot OH$	1.31×10^{-13}	0.48
$SO_4^{\cdot -}$	5.10×10^{-12}	0.19
$^1O_2$	1.89×10^{-9}	30.05
$O_2^{\cdot -}$	8.21×10^{-10}	69.28

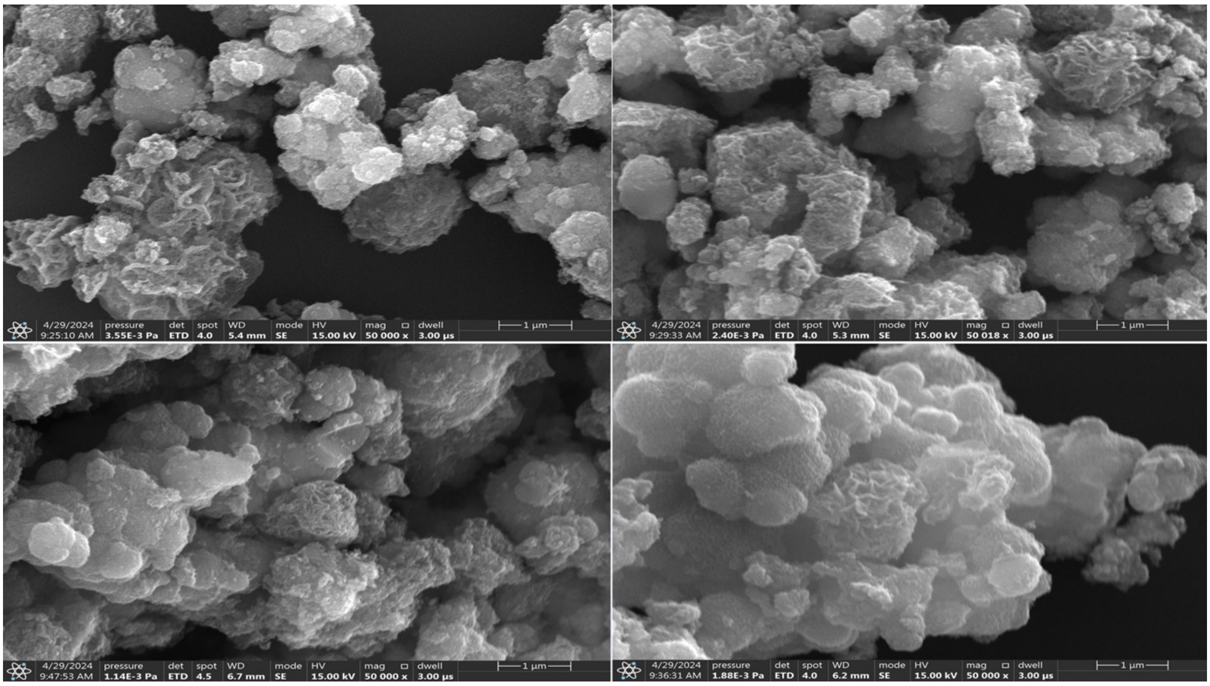

Figure S1. SEM images of Fe-Mn DAC.

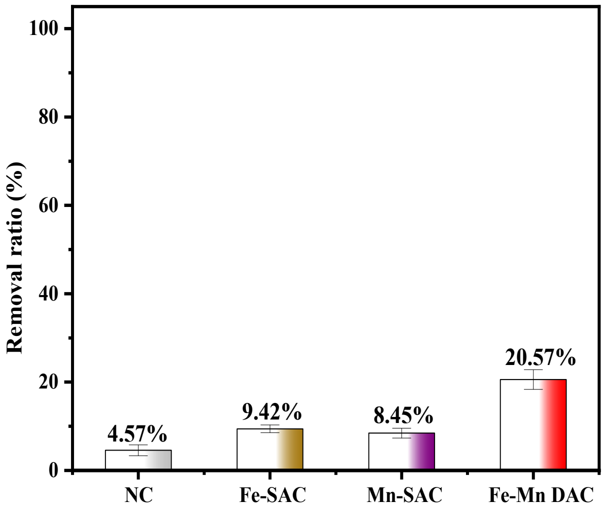

Figure S2. BPA adsorption on various catalysts in heterogeneous Fenton-like reaction. Reaction conditions: [BPA]=20 mg L^{-1}, [catalyst]=0.2 g L^{-1}, [PMS]=0.2 g L^{-1}, pH=7.0, T=25 ^{o}C, adsorption time=30 min.

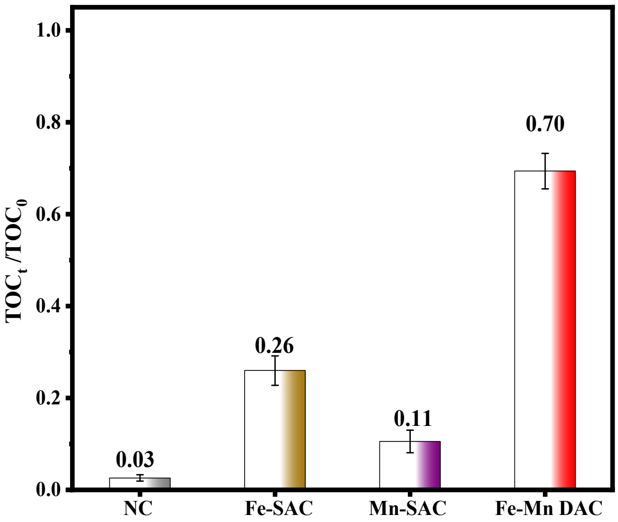

Figure S3. TOC removal by various catalysts in heterogeneous Fenton-like reaction. Reaction conditions: [BPA]=20 mg L^{-1}, [catalyst]=0.2 g L^{-1}, [PMS]=0.2 g L^{-1}, pH=7.0, T=25 ^{o}C, reaction time= 10 min.

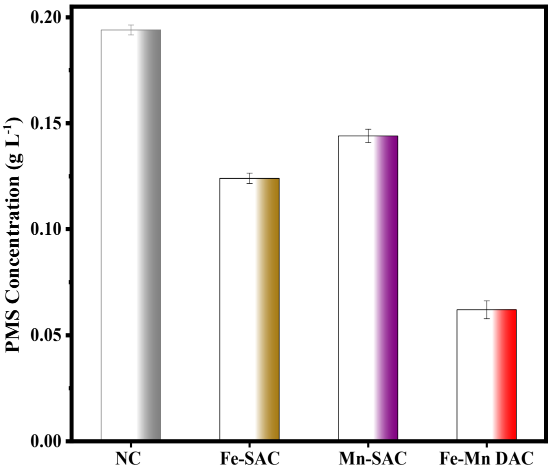

Figure S4. PMS consumption with various catalysts for BPA degradation in heterogeneous Fenton-like reaction. Reaction conditions: [BPA]=20 mg L^{-1}, [catalyst]=0.2 g L^{-1}, [PMS]=0.2 g L^{-1}, pH=7.0, T=25 ^{o}C, reaction time= 10 min.

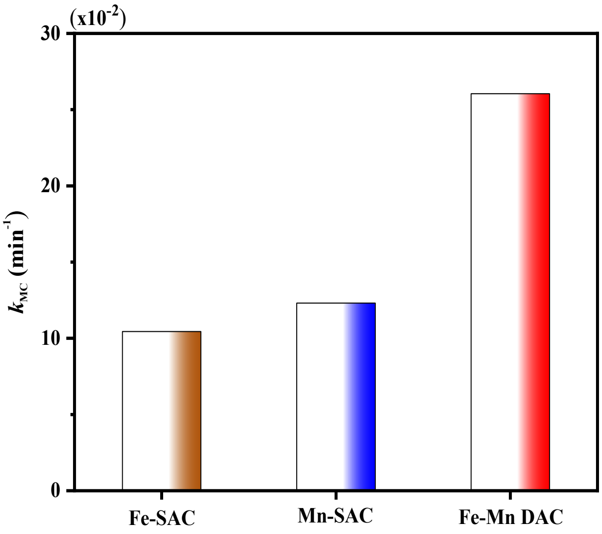

Figure S5. Comparison of normalized *k* to metal loading. Reaction conditions: [BPA]= 20 mg L^{-1}, [catalyst]=0.2 g L^{-1}, [PMS]=0.2 g L^{-1}, pH=7.0, T=25 ^{o}C.

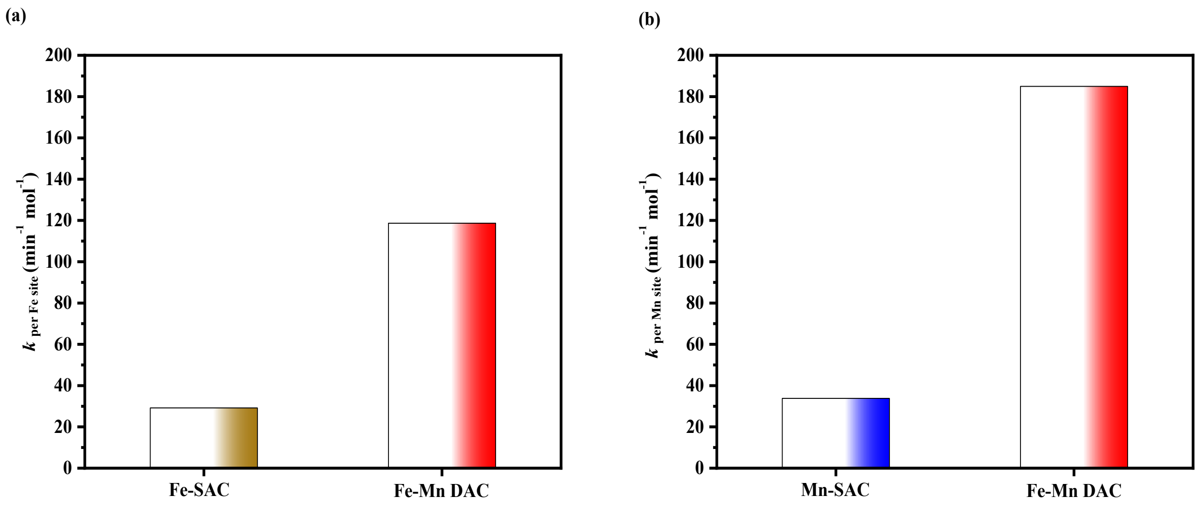

Figure S6. Comparison of normalized *k* to the molar ratio of metal loading per (a) Fe site and (b) Mn site. Reaction conditions: [BPA]= 20 mg L^{-1}, [catalyst]=0.2 g L^{-1}, [PMS]=0.2 g L^{-1}, pH=7.0, T=25 ^{o}C.

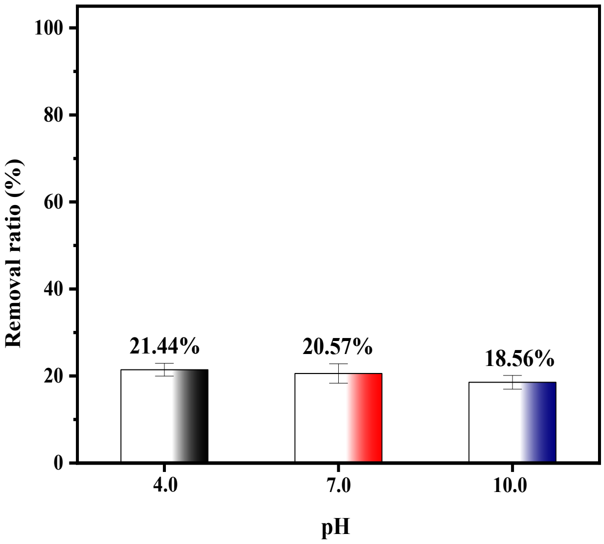

Figure S7. Effect of pH on the BPA adsorption in Fe-Mn DAC/PMS system. Reaction conditions: [BPA]=20 mg L^{-1}, [catalyst]=0.2 g L^{-1}, [PMS]=0.2 g L^{-1}, T=25 °C, adsorption time=30 min.

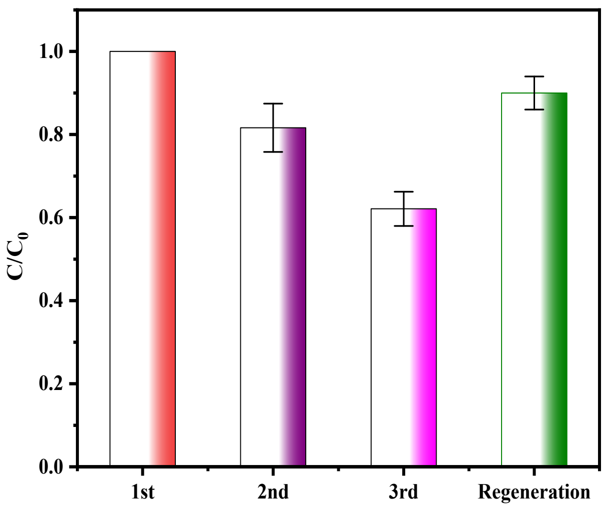

Figure S8. Stability test of Fe-Mn DAC for BPA degradation. Reaction conditions: [BPA]=20 mg L^{-1}, [catalyst]=0.2 g L^{-1}, [PMS]=0.2 g L^{-1}, pH=7.0, T=25 ^{o}C, reaction time=30 min.

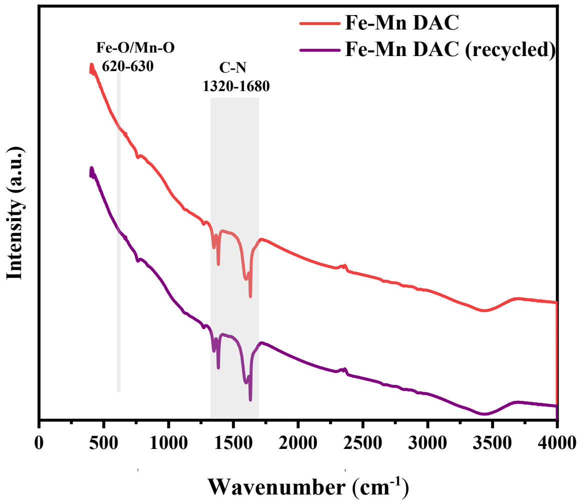

Figure S9. FTIR spectrum of transmittance of fresh and recycled Fe-Mn DAC.

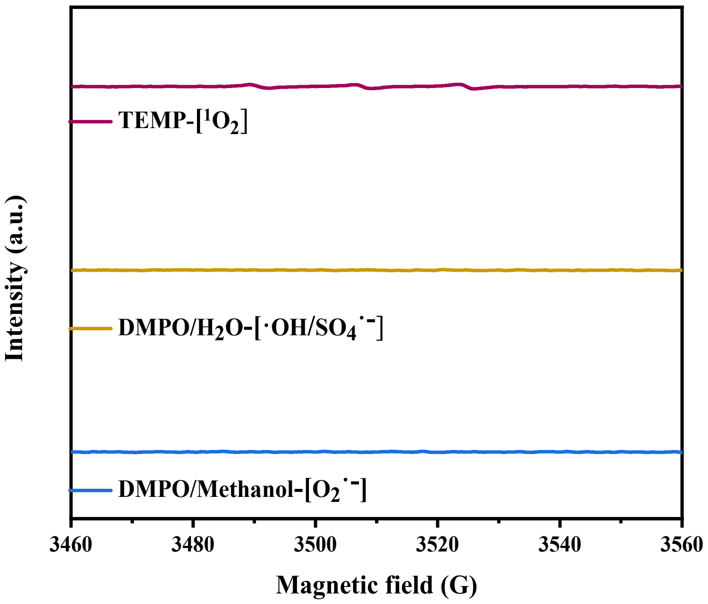

Figure S10. EPR spectra in PMS alone.

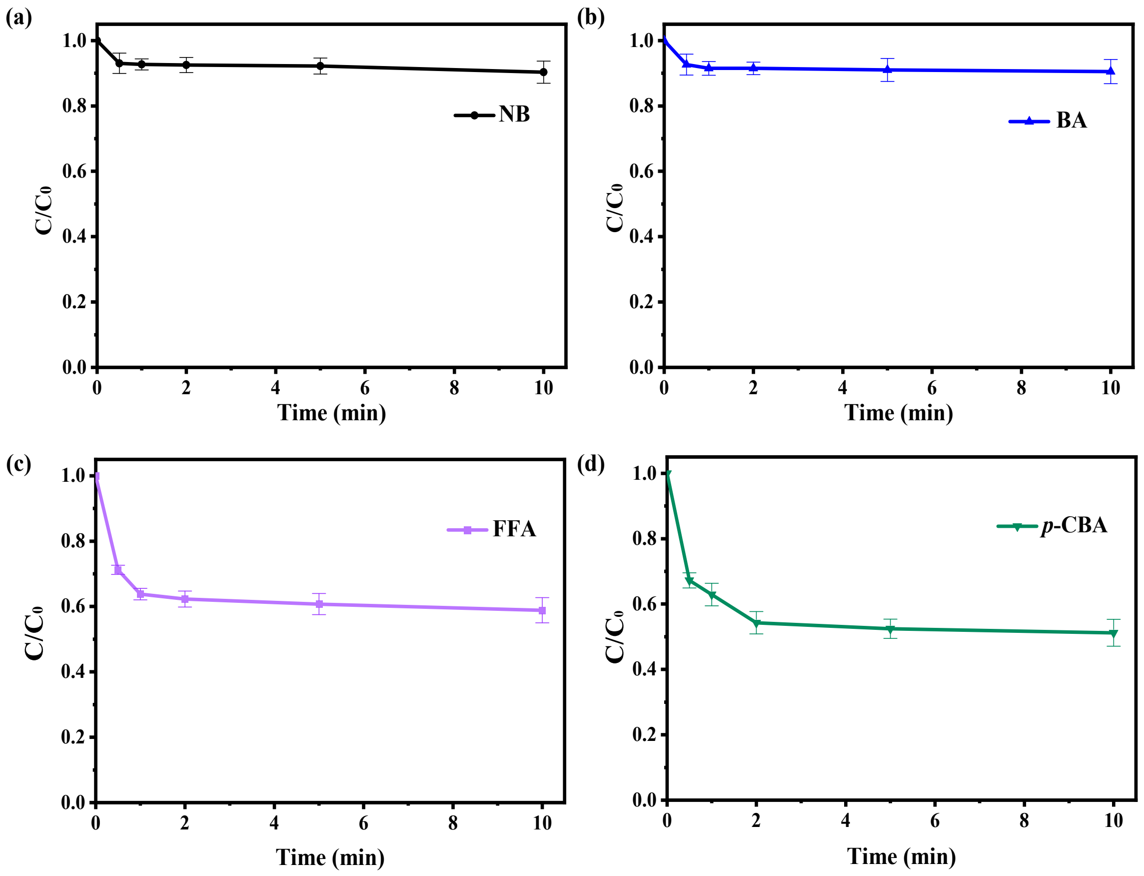

Figure S11. (a) NB, (b) BA, (c) FFA, and (d) *p*-CBA degradation efficiency in Fe-Mn DAC/PMS system. Reaction conditions: [BPA]=20 mg L^{-1}, [catalyst]=0.2 g L^{-1}, [PMS]=0.2 g L^{-1}, pH=7.0, T=25 ^{o}C , [probe]= 2.0 mg L^{-1}.

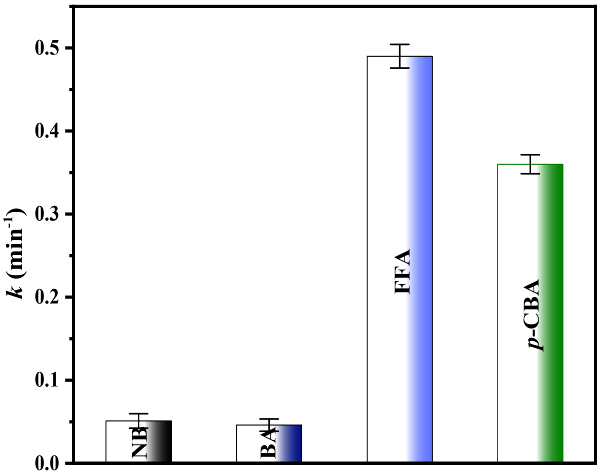

Figure S12. *k* of NB, BA, FFA, and *p*-CBA degradation efficiency in Fe-Mn DAC/PMS system. Reaction conditions: [BPA]=20 mg L^{-1}, [catalyst]=0.2 g L^{-1}, [PMS]=0.2 g L^{-1}, pH=7.0, T=25 ^{o}C , [probe]= 2.0 mg L^{-1}.

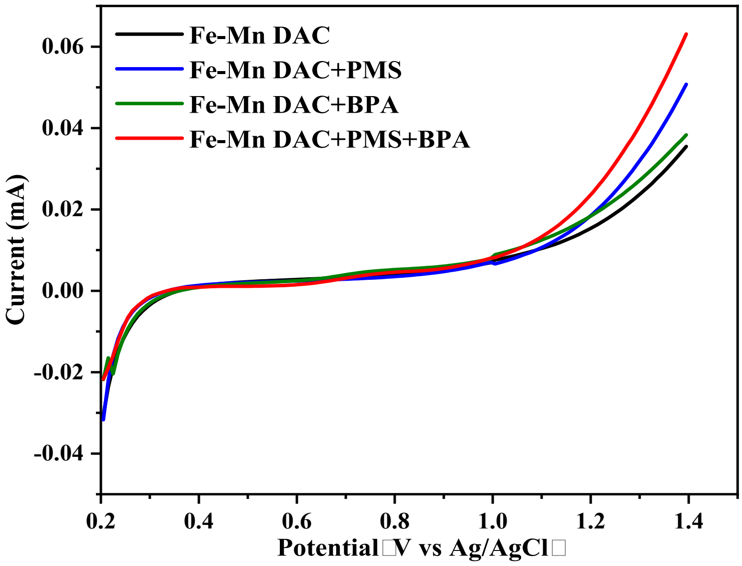

Figure S13. Linear sweep voltammetry obtained by Fe-Mn DAC as a working electrode in the presence of PMS and BPA.

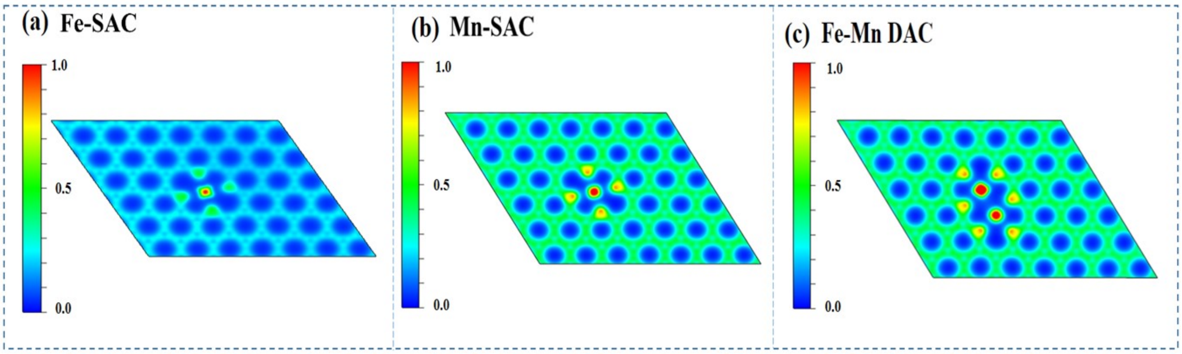

Figure S14. 2-D electron density distribution structure of (a) Fe-SAC, (b) Mn-SAC, and (c) Fe-Mn DAC.

Figure S15. Charge density difference (top view) in a PMS molecule adsorbed on (a) Fe–SAC, (b) Mn-SAC, (c) Fe-Mn DAC $_{\text{(Fe site)}}$, and (d) Fe-Mn DAC $_{\text{(Mn site)}}$.

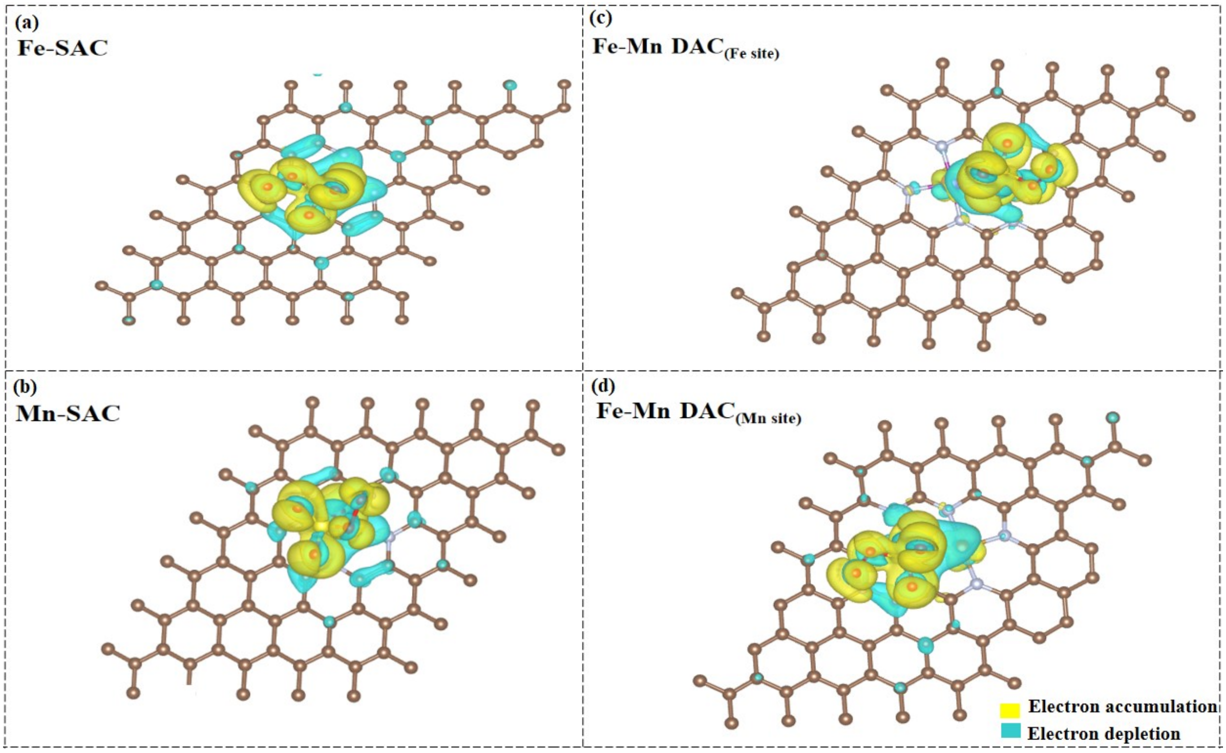

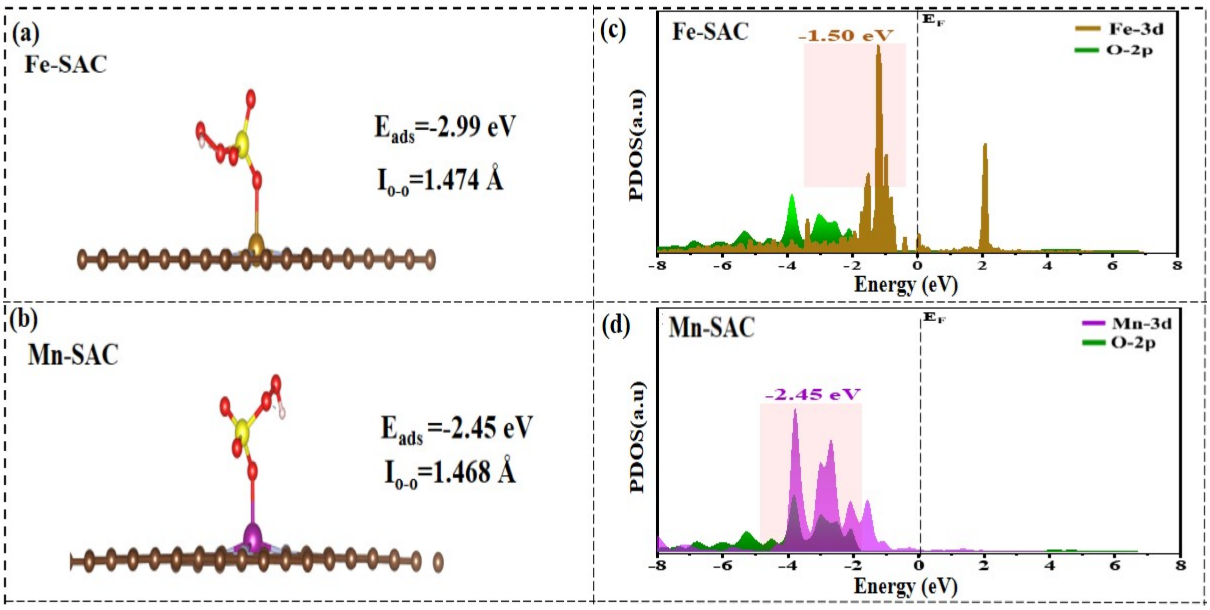

Figure S16. DFT calculations of PMS adsorption and activation on Fe-SAC and Mn-SAC. Representation of PMS molecule, adsorption energy, and O-O bond stretching on (a) Fe-SAC and (b) Mn-SAC, PDOS of (c) Fe-SAC and (d) Mn-SAC.

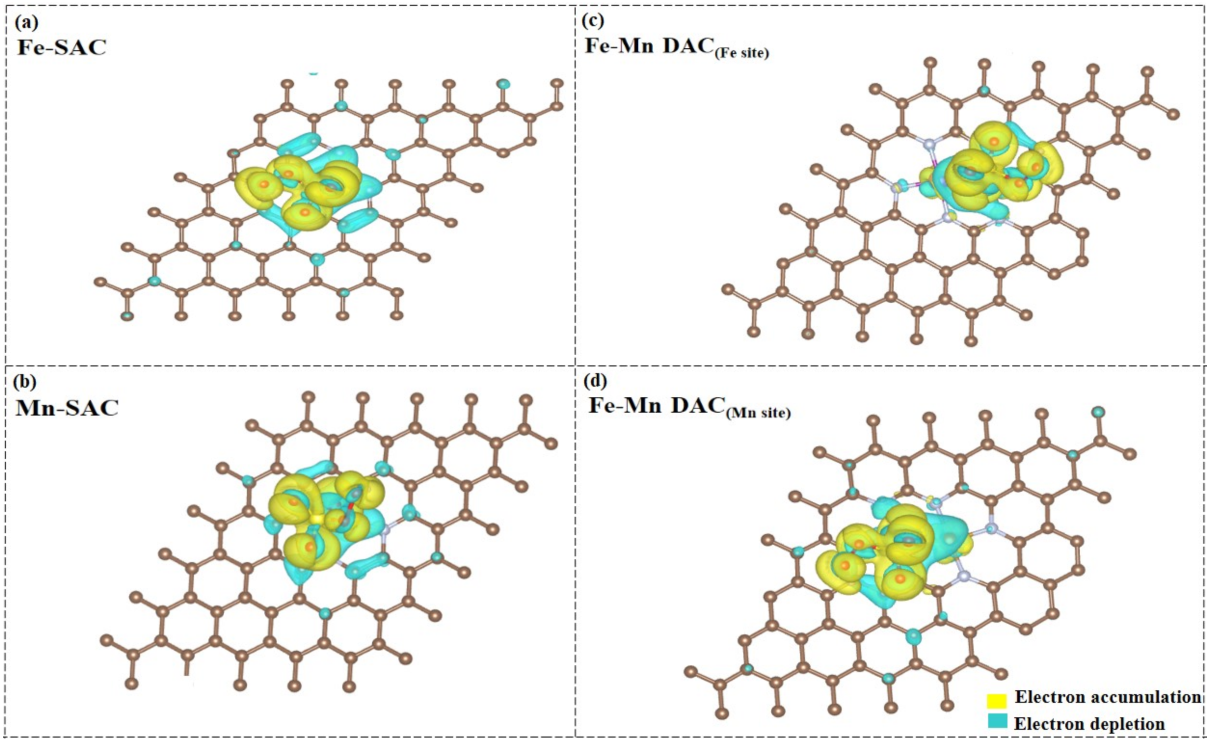

Figure S17. Bader charges on (a) Fe-SAC, (b) Mn-SAC, (c) Fe-Mn DAC $_{\text{(Fe site)}}$, and (d) Fe-Mn DAC $_{\text{(Mn site)}}$.

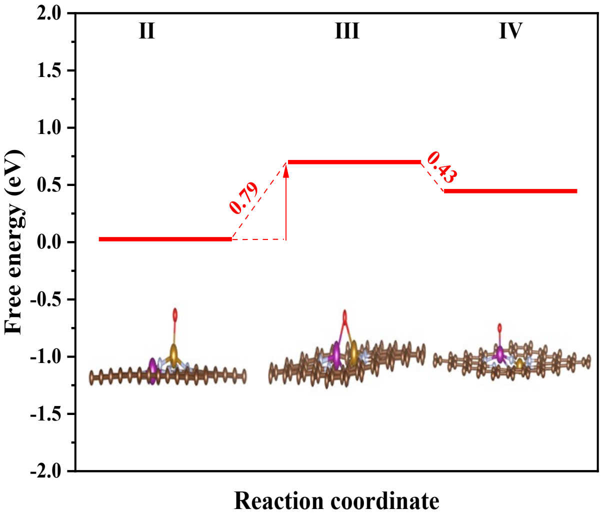

Figure S18. Free energy of O transfer in Fe-Mn DAC/PMS system.

References:

[1] Zhao Z, Hu M, Nie T, Zhou W, Pan B, Xing B, Zhu L. Improved electronic structure from spin-state reconstruction of a heteronuclear Fe–Co diatomic pair to boost the Fenton-like reaction. *Environ. Sci. Technol*. 2023;57:4556–4567.

[2] Miao J, Song J, Lang J, Zhu Y, Dai J, Wei Y, Long M, Shao Z, Zhou B, Alvarez PJ, Zhang L. Single-Atom MnN_5 catalytic sites enable efficient peroxymonosulfate activation by forming highly reactive Mn(IV)–oxo species. *Environ. Sci. Technol*. 2023;57:4266–4275.

[3] Huang B, Wu Z, Wang X, Song X, Zhou H, Zhang H, Zhou P, Liu W, Xiong Z, Lai B. Coupled surface-confinement effect and pore engineering in a single-Fe-atom catalyst for ultrafast Fenton-like reaction with high-valent iron-oxo complex oxidation. *Environ. Sci. Technol*. 2023;57:15667–15679.

[4] Long Y, Cao Z, Wu W, Liu W, Yang P, Zhan X, Chen R, Liu D, Huang W. Rational modulation of Fe single-atom electronic structure in a Fe–N_2B_4 configuration for preferential $^1O_2$ generation in Fenton-like reactions. *Appl. Catal. B Environ*. 2024;344:123643.

[5] Wang F, Gao Y, Fu H, Liu SS, Wei Y, Wang P, Zhao C, Wang JF, Wang CC. Almost 100% electron transfer regime over Fe–Co dual-atom catalyst toward pollutants removal: regulation of peroxymonosulfate adsorption mode. *Appl. Catal. B Environ*. 2023;339:123178.

[6] Zhang B, Li X, Bingham PA, Akiyama K, Kubuki S. Carbon matrix with atomic dispersion of binary cobalt/iron-N sites as efficient peroxymonosulfate activator for organic pollutant oxidation. *Chem. Eng. J*. 2023;451:138574.

[7] Sun J, Zhang D, Xia D, Li Q. Orange peels biochar doping with Fe–Cu bimetal for PMS activation on the degradation of bisphenol A: a synergy of SO_4^{2-}, •OH, $^1O_2$ and electron transfer. *Chem. Eng. J*. 2023;471:144832.

[8] Yang T, Fan S, Li Y, Zhou Q. Fe–N/C single-atom catalysts with high density of Fe–N_x sites toward peroxymonosulfate activation for high-efficient oxidation of bisphenol A: electron-transfer mechanism. *Chem. Eng. J*. 2021;419:129590.

[9] Zhang L-S, Jiang X-H, Zhong Z-A, Tian L, Sun Q, Cui Y-T, Lu X, Zou J-P, Luo S-L. Carbon nitride supported high-loading Fe single-atom catalyst for activation of peroxymonosulfate to generate $^1O_2$ with 100% selectivity. *Angew. Chem. Int. Ed*. 2021;60:21751–21755.

[10] Zhou X, Ke M-K, Huang G-X, Chen C, Chen W, Liang K, Qu Y, Yang J, Wang Y, Li F, Yu H-Q, Wu Y. Identification of Fenton-like active Cu sites by heteroatom modulation of electronic density. *Proc. Natl. Acad. Sci. U.S.A*. 2022;119:e2119492119.

[11] Chu C, Yang J, Zhou X, Huang D, Qi H, Weon S, Li J, Elimelech M, Wang A, Kim J-H. Cobalt single atoms on tetrapyridomacrocyclic support for efficient peroxymonosulfate activation. *Environ. Sci. Technol*. 2021;55:1242–1250.

[12] Qi Y, Li J, Zhang Y, Cao Q, Si Y, Wu Z, Akram M, Xu X. Novel lignin-based single atom

catalysts as peroxymonosulfate activator for pollutants degradation: role of single cobalt and electron transfer pathway. *Chem. Eng. J.* 2021;286:119910.

[13] Li Y, Yang T, Qiu S, Lin W, Yan J, Fan S, Zhou Q. Uniform N-coordinated single-atomic iron sites dispersed in porous carbon framework to activate PMS for efficient BPA degradation via high-valent iron-oxo species. *Chem. Eng. J.* 2020;389:124382.

[14] Yang M, Hou Z, Zhang X, Gao B, Li Y, Shang Y, Yue Q, Duan X, Xu X. Unveiling the origins of selective oxidation in single-atom catalysis via Co–N_4–C intensified radical and nonradical pathways. *Environ. Sci. Technol.* 2022;56:11635–11645.

[15] You J, Zhang C, Wu Z, Ao Z, Sun W, Xiong Z, Su S, Yao G, Lai B. N-doped graphite encapsulated metal nanoparticles catalyst for removal of Bisphenol A via activation of peroxymonosulfate: a singlet oxygen-dominated oxidation process. *Chem. Eng. J.* 2021;415:128890.

[16] Oh W-D, Dong Z, Hu Z-T, Lim T-T. A novel quasi-cubic $CuFe_2O_4$–Fe_2O_3 catalyst prepared at low temperature for enhanced oxidation of bisphenol A via peroxymonosulfate activation. *J. Mater. Chem. A*. 2015;3:22208–22217.

[17] Oh W-D, Lua S-K, Dong Z, Lim T-T. High surface area DPA-hematite for efficient detoxification of bisphenol A via peroxymonosulfate activation. *J. Mater. Chem.* 2014;15836–15845.

[18] Hu L, Zhang G, Wang Q, Sun Y, Liu M, Wang P. Facile synthesis of novel Co_3O_4-Bi_2O_3 catalysts and their catalytic activity on bisphenol A by peroxymonosulfate activation. *Chem. Eng. J.* 2017;326:1095–1104.

[19] Huang G-X, Wang C-Y, Yang C-W, Guo P-C, Yu H-Q. Degradation of bisphenol A by peroxymonosulfate catalytically activated with $Mn_{1.8}Fe_{1.2}O_4$ nanospheres: synergism between Mn and Fe. *Environ. Sci. Technol.* 2017;51:12611–12618.

[20] Li X, Wang Z, Zhang B, Rykov AI, Ahmed MA, Wang J. $FexCo_{3-x}O_4$ nanocages derived from nanoscale metal–organic frameworks for removal of bisphenol A by activation of peroxymonosulfate. *Appl. Catal. B Environ*. 2016;181:788–799.

[21] Gao Y, Zhu Y, Lyu L, Zeng Q, Xing X, Hu C. Electronic structure modulation of graphitic carbon nitride by oxygen doping for enhanced catalytic degradation of organic pollutants through peroxymonosulfate activation. *Environ. Sci. Technol.* 2018;52:14371–14380.

[22] Wang Y, Cao D, Liu M, Zhao X. Insights into heterogeneous catalytic activation of peroxymonosulfate by Pd/g-C_3N_4: the role of superoxide radical and singlet oxygen. *Catal. Commun*. 2017;102:85–88.

[23] Wang Y, Zhao X, Cao D, Wang Y, Zhu Y. Peroxymonosulfate enhanced visible light photocatalytic degradation of bisphenol A by single-atom dispersed Ag mesoporous g-C_3N_4 hybrid. *Appl. Catal. B Environ*. 2017;211:79–88.

[24] Lin K-YA, Zhang Z-Y. Degradation of bisphenol A using peroxymonosulfate activated by

one-step prepared sulfur-doped carbon nitride as a metal-free heterogeneous catalyst. *Chem. Eng. J*. 2017;313:1320–1327.